Solving Helmholtz problem with a fast numerical strategy based on Toeplitz structure

Manel L. Amamou

Faculty of Science Mathematics Physics and Natural of Tunis, University Tunis-El Manar

amamou.manel@gmail.com

ABSTRACT

This paper develops primarily an analytical solution for sound, electromagnetic or any other wave propagation described by the Helmholtz equation in the case of N circular obstacles. Then, it proposes a fast iterative numerical method, using Toeplitz block structure, for computing the solution of a complex, dense and large linear system. Finally, it shows the efficiency of this numerical strategy via a numerical study of the convergence rate with respect to different geometrical parameters of the problem.

Keywords:

Helmholtz equation; Toeplitz matrix; complex linear system; numerical strategy.

Council for Innovative Research

Peer Review Research Publishing System

1. INTRODUCTION

Waves are interesting physical phenomena with important practical applications. Physicists and engineers are interested in the reliable simulation of processes in which waves are scattered from obstacles (Scattering problems).

"Multiple scattering" means different things to different scientists, but a general definition might be "the interaction of fields with two or more obstacles" [16]. The problem of solving multiple scattering problems efficiently has received considerable attention in a broad rang of areas of applied sciences like acoustics, electromagnetism, elasticity and marine engineering. The aim of these research efforts is to devise efficient and robust numerical methods which allow the study of the scattering behaviour of general configurations of arbitrary shaped obstacles.

In many cases the obstacles are circular, or can be modeled as such. For example, we are exploring the modeling of the human head and body using two circular disks representing the head and the torso respectively. In fluid mechanical problems, bubbles or dust particles can be assumed circular. A typical multiple-scattering problem in classical physics is the scattering of sound waves by two rigid spheres. Further examples, such as the scattering of spherical electron waves by a cluster of atoms, can be found in condensed-matter physics [5,11,12, 13]. The scattering field in a multiple-scattering problem results from the complex interaction between the incident excitation fields and the separate obstacles on the one hand and between the different scatterers on the other hand. The strength and nature of these interactions depend largely on the shape and surface properties of the obstacles, their relative position with respect to each other and the physical proprieties of the surronding medium. Due to the complex nature of these phenomena, the development of numerical methods to study this type of problems requires special attention, especially when a large number of obstacles is present and/or when the frequency of interest is high. The waves scattered by a single obstacle can be calculated in various well-known ways, such as by the variables separation methods, T-matrix methods or integral-equation methods, which are discussed in detail by Martin [16].

For instance, Zaviska considered multiple scattering from an array of parallel circular cylinders [22]. He derived an infinite linear system or the unknown Fourier coefficients of the scattered field, which involve Fourier expansions of the purely outgoing wave fields about individual cylindrical obstacles. Unlike the case of one object where the Mie series solution expressed by the Fourier coefficients is explicitly obtained through the inversion of a diagonal matrix, the case of multiple scattering is more complex and requires the use of numerical methods. Indeed, it can be shown that the scattered field admits an expansion of a superposition of Fourier series. Therefore, the set of Fourier coefficients is the solution of a non-diagonal and dense complex linear system which can be extremely large for many obstacles at high-frequency. The numerical solution of this system has been already obtained by some authors [19, 20, 21, 23, 14]. However, this method remains restricted to low- and mid-frequencies. Alternative solutions using a generic numerical methodology based on a "multi-level" modeling approach are proposed by Genechten et al. [10], the generic character of the method is achieved by integrating the multiple-scatterer interactions in an exiting numerical modeling frame work. This is applicable to the study of a configuration of well separated obstacles of arbitrary shape on which any type of acoustic boundary condition can be applied. However, this method is applied to low and mid- wave numbers.

For multiple scattering problems with high-frequency Ecevit and Reitich [9] present an analysis of a recently proposed integral-equation method for the solution of electromagnetic and acoustic scattering problems. It delivers error-controllable solutions in frequency-independent computational times. Antoine et al. [1] analyzed numerically the problem for a two-dimensional case and for circular objects of the same sizes. However, Bruno and co-authors [3-4] analysed the multiple scattering problem for two- and three-dimensional cases by convex and non convex objects. The present paper focuses on the scattering problem by circular obstacles using the multipole expansion and on developing a reliable and robust accurate numerical solution for high frequencies and for many circular objects of different sizes.

The outline of the paper is organized as follows:

Section 2: We present the statement of the scattering problem by N circular disjoint obstacles situated in a homogenous acoustic medium.

Section 3: We recall some classical results using multipole expansion formulation for solving this kind of multiple scattering problems.

Section 4: We show that the Fourier coefficients of the local scattered field solve an infinite, complex, dense and large linear system (see (29)). Then, we explain how to truncate the above infinite system suitably to get an accurate numerical solution.

Section 5: We reduce the memory storage and accelerate the computation of the matrix vector product of the linear system by using Toeplitz structure. Then, we present a numerical study of the convergence rate with respect to different geometrical parameters of the problem.

Section 6: We conclude by summing up our results.

2. STATEMENT OF THE PROBLEM

Consider the problem of sound scattering by N disjoint scatterers $S_1,...,S_N$ with radii $a_1,...,a_N$ and situated in an homogeneous acoustic medium filling the whole space R. We denote by $\Omega_- = \cup_{p=1}^{N} S_p$ the domain occupied by the obstacles. The scattering problem in the frequency domain is reduced to solution of the Helmholtz equation for complex potential u(**r**),

$$\Delta u + k^2 u = 0, \tag{1}$$

with the following impedance boundary conditions on the surface S_p of the pth obstacle

$$\left(\alpha \frac{\partial u}{\partial n} + i\sigma u \right)\Big|_{S_p} = 0, \qquad p = 1, \dots, N \tag{2}$$

where k is the wavenumber, σ is a constant characterizing impedance of obstacle, α is a constant and $i^2 = -1$. In the particular case of sound-hard surfaces (σ=0 and α≠0), we have the Neumann boundary conditions,

$$\frac{\partial u}{\partial n}\Big|_{S_p} = 0, \tag{3}$$

and in the case of sound-soft surfaces (σ≠0 and α=0) we have the Dirichlet boundary conditions,

$$u|_{S_p} = 0, \tag{4}$$

In our work, we consider the scattering problem of an incident plane wave

$$u_{inc}(\mathbf{r}) = e^{(ik\beta.\mathbf{r})} \tag{5}$$

of direction β by Ω., where the time dependence is assumed to be of the form $e^{-i\omega\tau}$ and where the wavenumber k is real. Far from the region occupied by the obstacles the complex potential tends to the potential of the incident wave $u_{inc}(\mathbf{r})$

$$u(\mathbf{r})|_{r\to\infty} \to u_{inc}(\mathbf{r}). \tag{6}$$

Usually the potential is represented in the form

$$u(\mathbf{r}) = u_{inc}(\mathbf{r}) + u_{scat}(\mathbf{r}), \tag{7}$$

where $u_{scat}(\mathbf{r})$ is the potential of the scattered field. Far from the region occupied by the obstacles, the scattered field should satisfy the Sommerfeld radiation condition in two dimensions

$$\lim_{r\to\infty} r^{1/2} \left(\frac{\partial u_{scat}}{\partial r} - ik u_{scat} \right) = 0. \tag{8}$$

3. SOLUTION USING MULTIPOLE ESPANSION METHOD

3.1 Decomposition of the scattered field

Due to the linearity of the multiple scattering problem, we have the following result

Theorem 1 [2] Let $u_{scat}(\mathbf{r})$ be the solution of the multiple scattering problem. Then, the family of N coupled single scattering problems for $p = 1, \dots, N$:

$$(D^p) \begin{cases} \Delta u^p + k^2 u^p = 0 & (\mathbb{R}^2 \backslash \overline{S_p}) \\ \Lambda u^p = -\Lambda \left(u_{inc} + \sum_{q=1, q\neq p}^{N} u^q \right) & (\partial S_p) \\ \lim_{r\to\infty} r^{1/2} \left(\frac{\partial u^p}{\partial r} - ik u^p \right) = 0 \end{cases}$$

admits a unique solution u^p. Furthermore, the following decomposition holds

$$u_{scat}(\mathbf{r}) = \sum_{p=1}^{N} u^p(\mathbf{r}). \tag{9}$$

Where u^p can be thought of as the field scattered by the pth obstacle. Each potential u^p is regular outside the pth scatterer and satisfies the Sommerfeld radiation condition

$$\lim_{r\to\infty} r^{1/2} \left(\frac{\partial u^p}{\partial r} - ik u^p \right) = 0 \qquad \forall p = 1, \dots, N. \tag{10}$$

3.2 Notation

In this work, we are interested in the case of circular scattering obstacles S_p of centers $O_p = (x_p, y_p)$ and radii a_p. Any point M of the plane will be described by its cartesian coordinates (x, y) or by its polar coordinates (see Fig. 1).

$$\mathbf{r} = \overrightarrow{OM}, \qquad r = |\mathbf{r}|, \qquad \theta = Angle(Ox, \mathbf{r}).$$

We will also use in the sequel the local polar coordinates of the point M in the orthonormal system of coordinates associated to the obstacle p.

$$\mathbf{r}_p = \overrightarrow{O_p M}, \qquad r_p = |\mathbf{r}_p|, \qquad \theta_p = Angle(Ox, \mathbf{r}_p).$$

We set for all $p = 1, \ldots, N$:

$$\mathbf{b}_p = \overrightarrow{OO_p}, \qquad b_p = |\mathbf{b}_p|, \qquad \propto_p = Angle(Ox, \mathbf{b}_p).$$

And for all $q = 1, \ldots, N$ with $q \neq p$:

$$\mathbf{b}_{pq} = \overrightarrow{O_q O_p}, \qquad b_{pq} = |\mathbf{b}_{pq}|, \qquad \propto_{pq} = Angle(Ox, \mathbf{b}_{pq}).$$
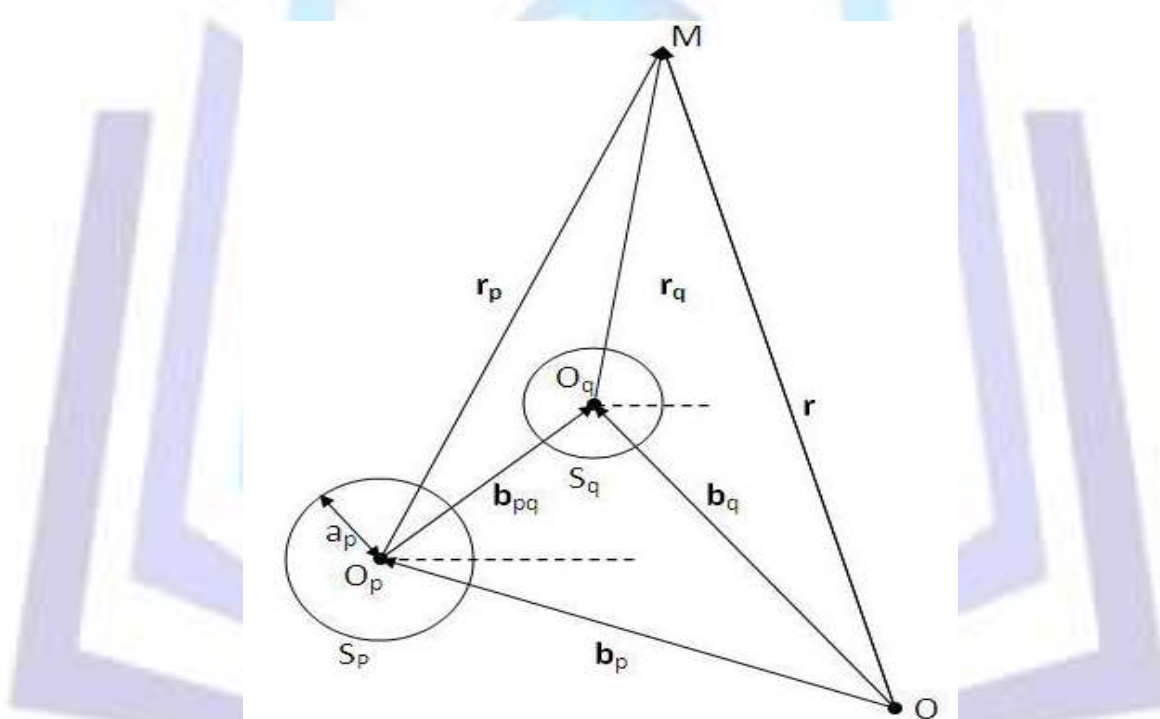

Figure 1: Notation for scattering by two circular obstacles.

3.3 Multipole expansion method

Definition 1 Let $r = (r\cos\theta, \ r\sin\theta)$. The outgoing cylindrical wavefunction ξ_n is defined by

$$\xi_n(\mathbf{r}) = H_n^{(1)}(kr)e^{in\theta} \qquad \forall n \in \mathbb{Z}.$$

Similarly, the regular cylindrical wavefunction $\hat{\xi}_n$ is defined by

$$\hat{\xi}_n(\mathbf{r}) = J_n(kr)e^{in\theta} \qquad \forall n \in \mathbb{Z},$$

Where J_n is the nth order Bessel function and $H_n^{(1)}$ is the nth order Hankel function of the first kind.

Definition 2 $\vee n \in \mathbb{Z}$ and for $p = 1, \ldots, N$, the local cylindrical wavefunctions associated with the obstacle p are defined by

$$\xi_n^p(\mathbf{r}) = \xi_n(\mathbf{r}_p) = H_n^{(1)}(kr_p)e^{in\theta_p}, \qquad \hat{\xi}_n^p(\mathbf{r}) = \hat{\xi}_n(\mathbf{r}_p) = J_n(kr_p)e^{in\theta_p}.$$

With the above notation, the incident wave can be expanded as

$$u_{inc}(\mathbf{r}) = \sum_{m \in \mathbb{Z}} d_m^p \, \hat{\xi}_m^p(\mathbf{r}), \tag{11}$$

where $d_m^p = e^{ik\beta.b_p} e^{im(\frac{\pi}{2}-\beta)}$, with $\beta = (\cos\beta, \sin\beta)$ describes the direction of the incident plane wave.

Similarly, the scattered field by the obstacle S_p can be expanded as

$$u_{scat}^p(\mathbf{r}) = \sum_{m \in \mathbb{Z}} x_m^p \xi_m^p(\mathbf{r}) \quad \forall p = 1, \dots, N, \qquad \forall r_p > a_p, \tag{12}$$

where the complex coefficients $\left(x_m^p\right)_{m \in \mathbb{Z}}$ are determined by imposing the boundary condition on the boundary of the obstacle p.

According relations (7) and (9), the complete potential can be expressed as follow

$$u(\mathbf{r}) = u_{inc}(\mathbf{r}) + \sum_{p=1}^N u_{scat}^p(\mathbf{r}) \tag{13}$$

and satisfies all the boundary conditions on the surface of each obstacle.

To solve this problem let us consider the pth obstacle. Near the center of this disk, all the potentials $u^q(\mathbf{r})$ are regular for $q \neq p$. Each $\xi_n^q(\mathbf{r})$ can be then re-expanded into a series as follows (see Ref. 16):

Theorem 2 [16] Let $1 \leq p, q \leq N$, with $q \neq p$. Then, we have the following relations

$$\xi_m^q(\mathbf{r}) = \begin{cases} \sum_{n \in \mathbb{Z}} S_{mn}(\mathbf{b}_{pq})\xi_n^p(\mathbf{r}), & r_p < b_{pq} \\ \sum_{n \in \mathbb{Z}} \hat{S}_{mn}(\mathbf{b}_{pq})\hat{\xi}_n^p(\mathbf{r}), & r_p > b_{pq} \end{cases} \tag{14}$$

where we have set

$$S_{mn}(\mathbf{b}_{pq}) = \xi_{m-n}(\mathbf{b}_{pq}) \quad \text{and} \quad \hat{S}_{mn}(\mathbf{b}_{pq}) = \hat{\xi}_{m-n}(\mathbf{b}_{pq}). \tag{15}$$

The infinite matrices $\mathbb{S}^{p,q} = \left(S_{mn}(\mathbf{b}_{pq})\right)_{m,n \in \mathbb{Z}}$ and $\hat{\mathbb{S}}^{p,q} = \left(\hat{S}_{mn}(\mathbf{b}_{pq})\right)_{m,n \in \mathbb{Z}}$ are called separation matrices as they depend on the distance b_{pq} between obstacles.

Substituting (11), (12) and the first equation in (14) into (13) we obtain the following representation of the field near the pth obstacle:

$$u(\mathbf{r}) = \sum_{m \in \mathbb{Z}} d_m^p \, \hat{\xi}_m^p(\mathbf{r}) + \sum_{m \in \mathbb{Z}} x_m^p \xi_m^p(\mathbf{r}) + \sum_{q=1,q \neq p}^N \sum_{m \in \mathbb{Z}} x_m^q \sum_{n \in \mathbb{Z}} S_{mn}(\mathbf{b}_{pq}) \xi_n^p(\mathbf{r}) \tag{16}$$

Let us change the order of summation in the latter term and substitute expressions for $\hat{\xi}_n^p(\mathbf{r})$ and $\xi_n^p(\mathbf{r})$ from definition 2, the expression (16) can be rewritten as

$$u(\mathbf{r}) = \sum_{m \in \mathbb{Z}} \left[x_m^p H_m^{(1)}(kr_p) + J_m(kr_p)\sum_{q=1,q \neq p}^N \sum_{n \in \mathbb{Z}} S_{nm}(\mathbf{b}_{pq})x_n^q + d_m^p J_m(kr_p)\right] e^{im\theta_p}. \tag{17}$$

3.4 Boundary conditions

From the last equation, we have the following relations for the boundary values of u and its normal derivative on the surface of the pth disk:

$$u|_{S_p} = \sum_{m \in \mathbb{Z}} \left[x_m^p H_m^{(1)}(ka_p) + J_m(ka_p)\sum_{q=1,q \neq p}^N \sum_{n \in \mathbb{Z}} S_{nm}(\mathbf{b}_{pq})x_n^q + d_m^p J_m(ka_p)\right] e^{im\theta_p}, \tag{18}$$

$$\frac{\partial u}{\partial n}\Big|_{S_p} = k \sum_{m \in \mathbb{Z}} \left[x_m^p H_m^{(1)\prime}(ka_p) + J_m'(ka_p)\sum_{q=1,q \neq p}^N \sum_{n \in \mathbb{Z}} S_{nm}(\mathbf{b}_{pq})x_n^q + d_m^p J_m'(ka_p)\right] e^{im\theta_p}. \tag{19}$$

Appling boundary condition (2) on the surface of the pth obstacle, we obtain

$$\sum_{m \in \mathbb{Z}} \left[\begin{array}{c} x_m^p\left(\alpha k \, H_m^{(1)\prime}(ka_p) + i\sigma H_m^{(1)}(ka_p)\right) \\ + \left(\alpha k J_m'(ka_p) + i\sigma J_m(ka_p)\right)\sum_{q=1,q \neq p}^N \sum_{n \in \mathbb{Z}} S_{nm}(\mathbf{b}_{pq})x_n^q + d_m^p\left(\alpha k J_m'(ka_p) + i\sigma J_m(ka_p)\right) \end{array} \right] e^{im\theta_p} = 0. \tag{20}$$

Orthogonality of $e^{im\theta_p}$ gives

$$x_m^p \left(\alpha k \, H_m^{(1)'}(ka_p) + i\sigma H_m^{(1)}(ka_p) \right)$$

$$+ \left(\alpha k \, J_m'(ka_p) + i\sigma J_m(ka_p) \right) \sum_{q=1, q\neq p}^{N} \sum_{n\in\mathbb{Z}} S_{nm}(\mathbf{b}_{pq}) x_n^q + d_m^p \left(\alpha k \, J_m'(ka_p) + i\sigma J_m(ka_p) \right) = 0. \tag{21}$$

Finally, $\forall m \in \mathbb{Z}$ and $\forall p = 1, \dots, N$, we have the following relation

$$x_m^p + \frac{\left(\alpha k \, J_m'(ka_p) + i\sigma J_m(ka_p) \right)}{\left(\alpha k \, H_m^{(1)'}(ka_p) + i\sigma H_m^{(1)}(ka_p) \right)} \sum_{q=1, q\neq p}^{N} \sum_{n\in\mathbb{Z}} S_{nm}(\mathbf{b}_{pq}) x_n^q = -d_m^p \frac{\left(\alpha k \, J_m'(ka_p) + i\sigma J_m(ka_p) \right)}{\left(\alpha k \, H_m^{(1)'}(ka_p) + i\sigma H_m^{(1)}(ka_p) \right)}. \tag{22}$$

For the particular case of sound-hard surfaces $(\sigma = 0 \text{ and } \alpha \neq 0)$ we have the equation associated to the Neumann boundary conditions, while for sound soft surfaces $(\sigma \neq 0 \text{ and } \alpha = 0)$ we obtain the equation associated to the Dirichlet boundary conditions.

4. MATRIX REPRESENTATION

4.1 Infinite linear system

Equation (22) forms an infinite linear system which can be written in the more compact matrix-vector form

$$\mathbb{X}^p + \mathbb{D}^p \sum_{q=1, q\neq p}^{N} (\mathbb{S}^{p,q})^T \mathbb{X}^q = \mathbb{Y}^p \qquad \forall p = 1, \dots, N, \tag{23}$$

where

- $\mathbb{X}^p = \left(x_n^p \right)_{n\in\mathbb{Z}}.$

- $(\mathbb{S}^{p,q})^T$ is the transpose of the separation matrix $\mathbb{S}^{p,q}$ defined by $\mathbb{S}^{p,q} = \left(\mathbb{S}_{mn}^{p,q} \right)_{m\in\mathbb{Z}, n\in\mathbb{Z}}$

  and $\mathbb{S}_{mn}^{p,q} = \xi_{m-n}(\mathbf{b}_{pq}).$

- $\mathbb{D}^p = \left(\mathbb{D}_{mn}^p \right)_{mn\in\mathbb{Z}}$ is the diagonal infinite matrix, with diagonal terms

$$\mathbb{D}_{m,m}^p = \frac{\alpha k \, J_m'(ka_p) + i\sigma J_m(ka_p)}{\alpha k \, H_m^{(1)'}(ka_p) + i\sigma H_m^{(1)}(ka_p)} \qquad \text{(Robin condition)}. \tag{24}$$

- $\mathbb{Y}^p = -\mathbb{D}^p \mathbf{d}^p$, where $\mathbf{d}^p = \left(d_m^p \right)_{m\in\mathbb{Z}}.$

The N infinite linear systems (23) can be written in the abstract form

$$\mathbb{A}\mathbb{X} = \mathbb{Y}, \tag{25}$$

where

$$\mathbb{A} = \begin{bmatrix} \mathbf{A}^{(11)} & \cdots & \mathbf{A}^{(1N)} \\ \vdots & \ddots & \vdots \\ \mathbf{A}^{(N1)} & \cdots & \mathbf{A}^{(NN)} \end{bmatrix}, \tag{26}$$

$$\mathbf{A}_{mn}^{(pq)} = \mathbb{D}_{mn}^p \left(\mathbb{S}_{mn}^{p,q} \right)^T, \quad \text{for } p \neq q \qquad \text{and} \qquad \mathbf{A}_{mn}^{(pq)} = \delta_{mn} \quad \text{for } p = q$$

δ_{mn} is the Kronecker delta, $\delta_{mn} = 0$ for $m \neq n$ and $\delta_{mn} = 1$ for $m = n$,

$$\mathbb{X} = \begin{bmatrix} \mathbf{X}^{(1)} \\ \mathbf{X}^{(2)} \\ \cdot \\ \cdot \\ \cdot \\ \mathbf{X}^{(N)} \end{bmatrix} \qquad \text{and} \qquad \mathbb{Y} = \begin{bmatrix} \mathbf{Y}^{(1)} \\ \mathbf{Y}^{(2)} \\ \cdot \\ \cdot \\ \cdot \\ \mathbf{Y}^{(N)} \end{bmatrix}.$$

4.2 Finite dimensional approximation

An important issue is the truncation of the infinite linear system (25) which corresponds to the truncation of the associated matrices. A first step is to select a number M_p of modes to retain for each expansion. We assume that we keep only the modes ξ_m^p such that $-M_p \leq m \leq M_p$, then the length of each vector $\mathbf{X}^{(p)}$ and $\mathbf{Y}^{(p)}$ will be $(2M_p + 1)$ and the size of each sub-matrix $\mathbf{A}^{(pq)}$ will be $(2M_p + 1) \times (2M_q + 1)$, the size of the total vectors $\mathbb{X}$ and $\mathbb{Y}$ will be $\sum_{p=1}^{N}(2M_p + 1)$ and the size of the total matrix $\mathbb{A}$ will be $\sum_{p=1}^{N}(2M_p + 1) \times \sum_{p=1}^{N}(2M_p + 1)$.

With this notation, (25) should be truncated to the finite system

$$X^p + D^p \sum_{q=1, q \neq p}^{N} (S^{p,q})^T X^q = Y^p \qquad \forall p = 1, \dots, N, \tag{27}$$

where

- $X^p = \left(x_n^p\right)_{n=-M_p, \dots, M_p},$

- $S^{p,q}$ is the $(2M_p + 1) \times (2M_q + 1)$ finite dimensional separation matrix.

- $D^p = \left(D_{mn}^p\right)_{-M_p \leq m \leq M_p, -M_q \leq n \leq M_q}$ is the diagonal infinite matrix, with diagonal terms

$$D_{m,m}^p = \frac{\alpha k\, J_m'(ka_p) + i\sigma J_m(ka_p)}{\alpha k\, H_m^{(1)'}(ka_p) + i\sigma H_m^{(1)}(ka_p)} \qquad \text{(Robin condition)}.$$

- $Y^p = -D^p \mathbf{d}^p$, where $\mathbf{d}^p = \left(d_m^p\right)_{-M_p \leq m \leq M_p}.$

The $\mathbb{N}$ coupled finite dimensional systems (27) can equivalently be written as

$$AX = Y, \tag{28}$$

Where $\mathbb{A}$ is the full complex square matrix of size $\sum_{p=1}^{N}(2M_p + 1) \times \sum_{p=1}^{N}(2M_p + 1)$ defined by

$$A = \begin{bmatrix} A^{(11)} & \cdots & A^{(1N)} \\ \vdots & \ddots & \vdots \\ A^{(N1)} & \cdots & A^{(NN)} \end{bmatrix}, \tag{29}$$

$$A_{mn}^{(pq)} = D_{mn}^p \left(S_{mn}^{p,q}\right)^T, \quad \text{for } p \neq q \qquad \text{and} \qquad A_{mn}^{(pq)} = \delta_{mn} \quad \text{for } p = q,$$

δ_{mn} is the Kronecker delta.

Two complex-valued vector fields

$$X = \begin{bmatrix} X^{(1)} \\ X^{(2)} \\ \cdot \\ \cdot \\ \cdot \\ X^{(N)} \end{bmatrix} \qquad \text{and} \qquad Y = \begin{bmatrix} Y^{(1)} \\ Y^{(2)} \\ \cdot \\ \cdot \\ \cdot \\ Y^{(N)} \end{bmatrix}.$$

For our simulations, the truncation number M_p is selected using the following formula

$$M_p = \left[ka_p + \left(\frac{1}{2\sqrt{2}} \ln\left(2\sqrt{2}\pi ka_p \epsilon^{-1}\right) \right)^{2/3} (ka_p)^{1/3} + 1 \right], \tag{30}$$

where $[y]$ denotes the integer part of a real number y, and ϵ is the desired error bound on the Fourier coefficients. The above formula has been proposed in the literature in the contexts of multipole methods [1,6] and single scattering [8].

5. NUMERICAL RESOLUTION OF THE PROBLEM

5.1 Geometrical configurations

In our numerical computations, we consider two kinds of geometrical configurations:

- *Single-row configuration*: This structure is composed of $N_x = N$ equally spaced obstacles aligned along the x-axis, the distance between two successive disks is denoted by δ, and $b_x = b_{12}$ denotes the distance separating the origins of two successive scatterers (see Fig. 2).
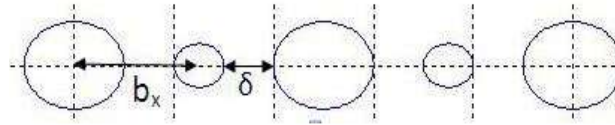

Figure 2: Single-row configuration with $N = N_x$ disks.

- *Rectangular configuration:* We consider here a rectangular lattice composed from $N = N_x \times N_y$ disks. We restrict our experiments to a rectangular lattice which is composed of N_y uniformly spaced single-rows with respect to $b_y = b_{1(N_x+1)}$, each row being composed from N_x equally spaced disks according to $b_x = b_{12}$ (see Fig. 3).
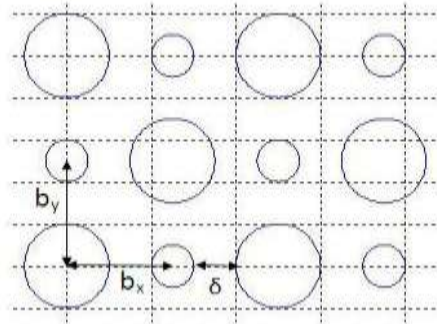
Figure 3: Rectangular configuration with $N = N_x \times N_y$ disks.

5.2 Compressed version of matrix

Matrix $\mathbb{A}$ has a particular structure. Each one of its off-diagonal blocks is obtained by multiplying the diagonal matrix $\mathbb{D}^p \in \mathbb{C}^{2M_p+1,2M_p+1}$ by the matrix $(\mathbb{S}^{p,q})^T \in \mathbb{C}^{2M_p+1,2M_q+1}$ which has a Toeplitz structure [7] since

$$\mathbb{S}^{p,q}_{mn} = \xi_{m-n}(\mathbf{b}_{pq}).$$

Definition 3 A Toeplitz matrix is a matrix of the type

$$T_n = \begin{bmatrix} h_0 & h_{-1} & \ldots & h_{2-n} & h_{1-n} \\ h_1 & h_0 & h_{-1} & \ddots & h_{2-n} \\ h_2 & h_1 & h_0 & \ddots & \vdots \\ \vdots & \ddots & \ddots & h_0 & h_{-1} \\ h_{n-1} & \ldots & h_2 & h_1 & h_0 \end{bmatrix}.$$

The generating vector

$$h = [h_{1-n}, h_{2-n}, \ldots, h_0, h_1, \ldots, h_{n-2}, h_{n-1}]^T \tag{31}$$

of $\mathbb{T}_n$ is called root vector.

A Toeplitz matrix is determined by its first row and first column.

Consequently, using the notation from Ref. [7], the storage of $(S^{p,q})^T$ can be optimized using a compressed version based on the root vector

$$h^{p,q} = \left[S^{p,q}_{M_q,-M_p}, \cdots, S^{p,q}_{-M_q+1,-M_p}, S^{p,q}_{-M_q,-M_p}, \cdots, S^{p,q}_{-M_q,M_p} \right]^T.$$

(32)

To show the improvement induced by the compressed storage version using (32) over the full version, we show in Fig. 4 the CPU time reduction with respect to the wavenumber k, to build the global matrix A compared to the compressed version in the single-row configuration with $N = 2$, $a_1 = 1$, $a_2 = 0.5$ and $\delta = 1.5$ for Robin problem $(\alpha = 1 \text{ and } \sigma = 1)$.
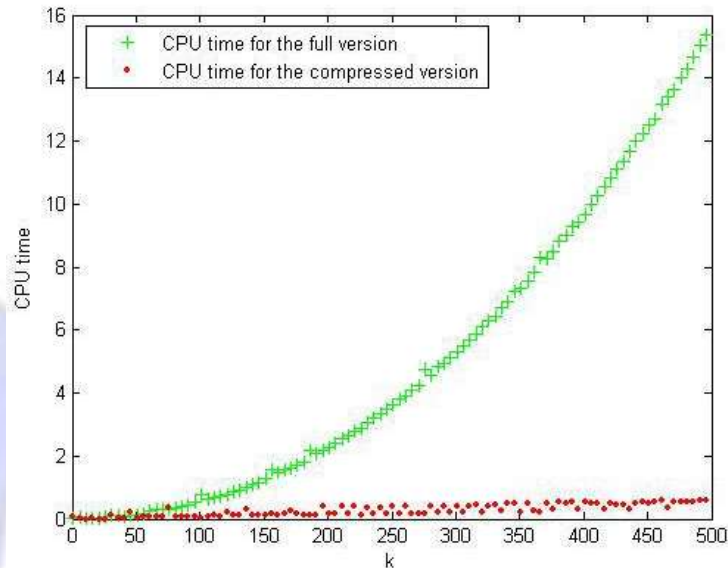
Figure 4: Variation of the CPU time in terms of the wavenumber k for building matrix A in the full and in the compressed version.

5.3 Iterative solver

The linear system (28) can be solved through an iterative linear solver [17,18]. We consider the GMRES, possibly with a restart parameter η, denoted by GMRES(η) [15]. The tolerance error of the iterative solver is set to tol and the number of iterations to get this tolerance is denoted by n[iter].

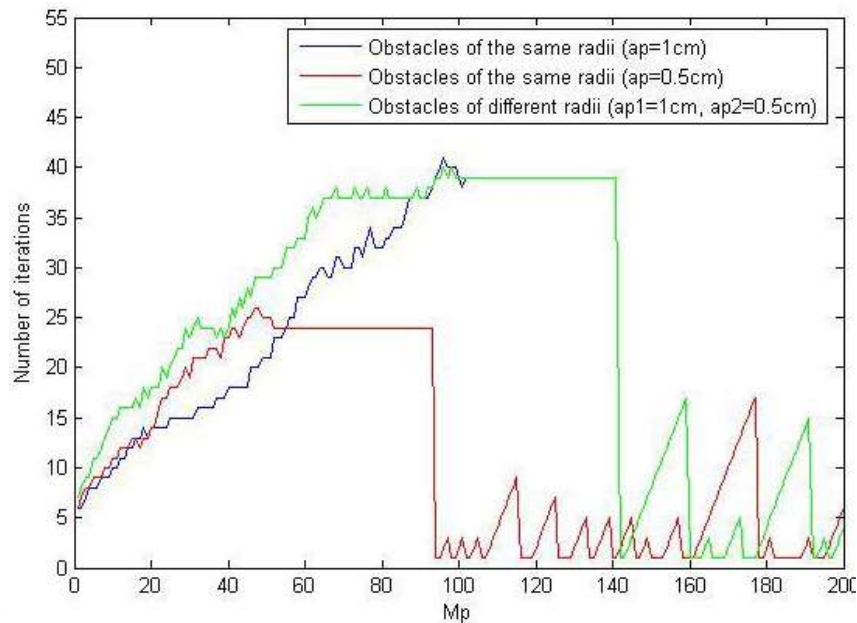We denote that all our numerical simulations and algorithms are developed under Matlab.

Figure 5: Variation of number of iterations in terms of truncation number M_p (Dirichlet problem).

5.3.1 Influence of the order of truncation M_p on the convergence

The order of truncation M_p must be fixed carefully e.g. through formula (30). M_p must be large enough to compute the solution accurately, but not too large to avoid the stagnation of the iterative solver. To make this statement precise, let us consider three different rectangular configurations: the first two form respectively a uniform square lattice with $a_p = 1$ and $a_p = 0.5$ for $1 \leq p \leq 4$ with $N_x = N_y = 2$ ($N = 4$) and $b_x = b_y = 3$, and the third one is composed of 4 obstacles of different radii $(a_1 = 1, a_2 = 0.5, a_3 = 0.5$ and $a_4 = 1)$, the wavenumber $k = 100$. The linear system (28) is solved by the GMRES with $tol = 10^{-8}$. For a given value of tol and along the paper, we fix $\varepsilon = tol$ in formula (30) and the angle of incidence $\beta = 0$.

Concerning the first two configurations, we report the number of iterations versus M_p. For a Dirichlet problem (see Fig. 5) we observe three distinct zones. First, from $M_p = 1$ to $M_p < ka_p (\forall a_p = 1$ or $a_p = 0.5$) the number of iterations increases. This means that the computation of a correct solution requires more harmonics.

This is obtained in the second stable zone for $ka_p \leq M_p \leq 140$ of rectangular lattice with scatterers of the same radii $a_p = 1$ and $ka_p \leq M_p \leq 92$ for $a_p = 0.5$. However, if we include too many harmonics (third zone), typically $M_p \geq 141$ for $a_p = 1$ and $M_p \geq 93$ for $a_p = 0.5$ we obtain a break down of the GMRES as can be remarked in Fig. 5, also in Fig. 6 where we represent the relative error with respect to M_p.
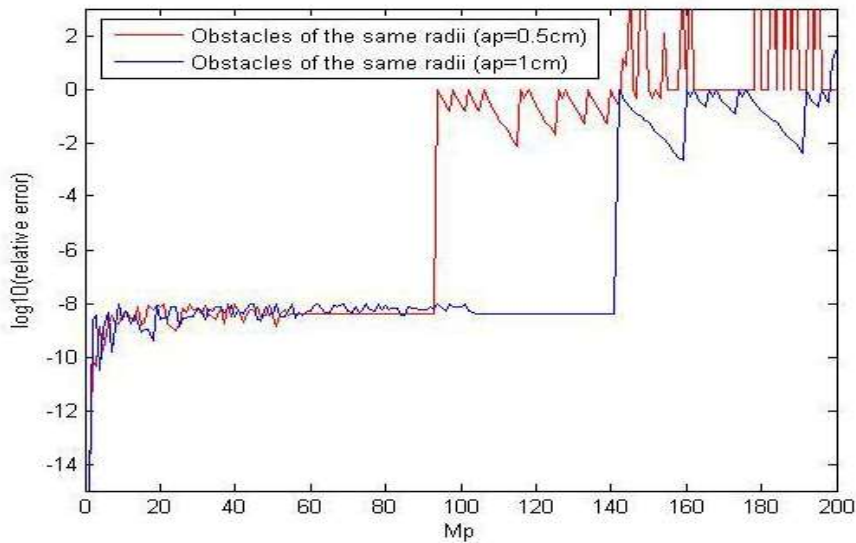
Figure 6: Variation of relative error in terms of truncation number M_p (Dirichlet problem).

We notice the same remarks for a Neumann problem (see Fig. 7 and Fig. 8), only for this kind of problem of sound-hard obstacles the stable zone is wider than that of sound-soft obstacles. According to the truncation formula (30) and for obstacles with the same radius $a_p = 0.5$, we have $M_p = 66$. So it is better to study a Dirichlet problem and estimate that $M_p \in [ka_p, 92]$ than to study a Neumann problem and estimate that $M_p \in [ka_p, 135]$. Moreover, for a rectangular configuration with sound-soft obstacles of different radii $(a_{p1} = 1$ and $a_{p2} = 0.5)$ we observe two distinct stable zones: The first one for $64 \leq M_p \leq 92$ and the second one for $100 \leq M_p \leq 140$ (see Fig. 5), which is not the case for Neumann problem (see Fig. 7). Even more, for a rectangular configuration with scatterers of different radii we represent the evolution of the residuals with respect to the number of iterations for $M_p = 66$, $M_p = 120$ and $M_p = 150$ (see Fig. 9). We notice the convergence of the iterative solver for $M_p = 66$ corresponding to obstacles with radii $a_p = 0.5$ and $M_p = 120$ for obstacles with radii $a_p = 1$. In contrast we observe the stagnation of the solver for $M_p = 150$, which is not the case for Neumann problem (see Fig. 10).
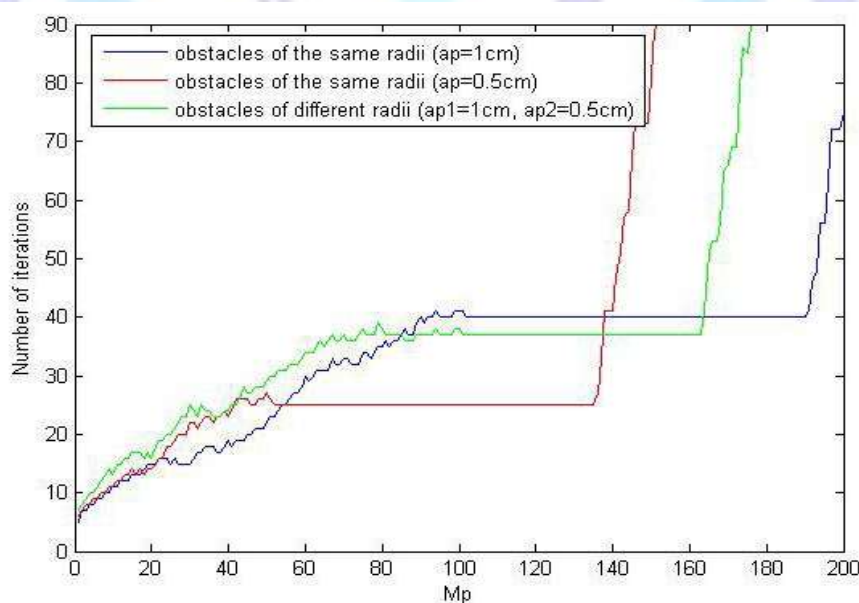

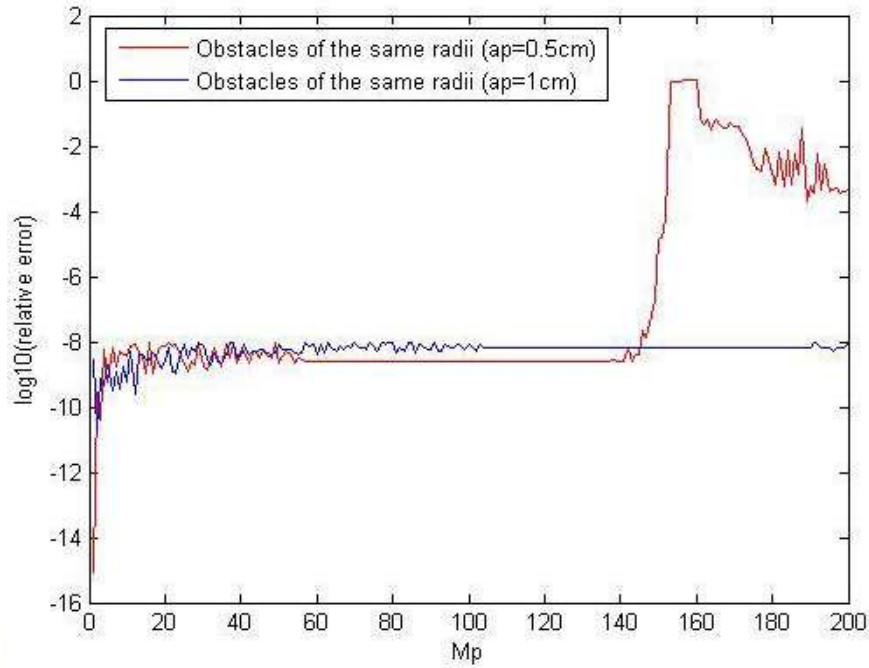**Figure 7: Variation of number of iterations in terms of truncation number M_p (Neumann problem).**

Figure 8: Variation of relative error in terms of truncation number M_p (Neumann problem).
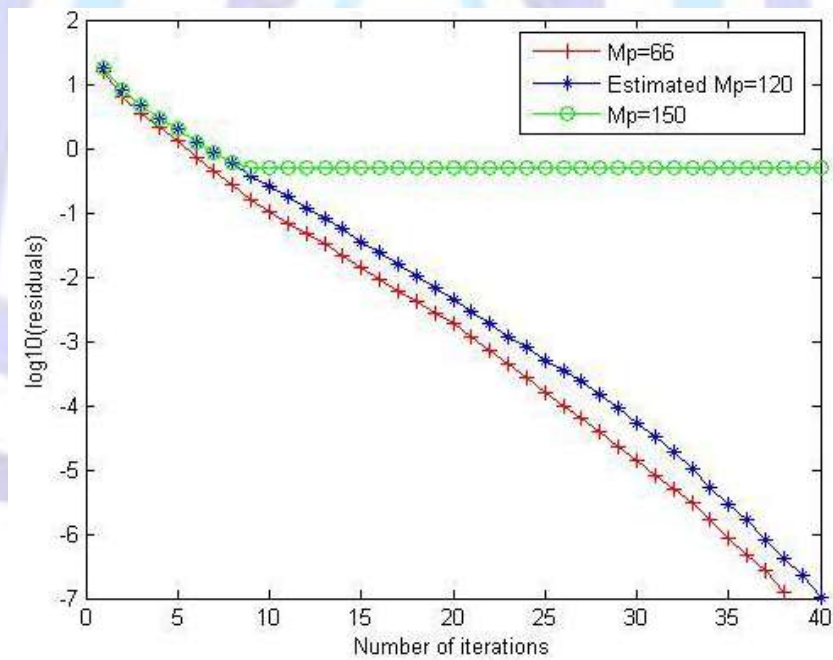

Figure 9: Variation of residuals in terms of number of iterations $M_p = 150$, $M_p = 120$ and $M_p = 66$ (Dirichlet problem).
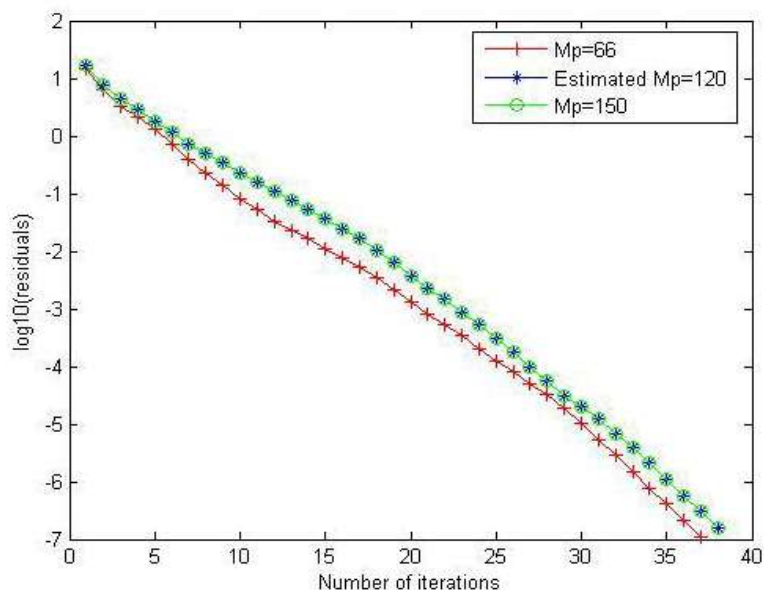
Figure 10: Variation of residuals in terms of number of iterations $M_p = 150$, $M_p = 120$ and $M_p = 66$

(Neumann problem).

If we summarize, a representation of the number of iterations with respect to M_p gives the following ideas: The first one concerns the size of scatterers. In fact, the number of iterations increases with the size of obstacles. The second is about the nature of the configuration which is uniform (with the same radii) and not uniform (with different radii). Finally, we notice that the choice of the truncation formula (30) is better used for the Dirichlet problem (Sound-soft obstacles) than the Neumann problem (Sound-hard obstacles). For this reason, from now, we restrict our numerical simulations to the Dirichlet case.

5.3.2 Fast matrix vector-product (MVP) for Toeplitz matrices

Let us recall that the main CPU cost of the GMRES is due to one matrix-vector product (MVP) per iteration. But to calculate the matrix-vector product we can use two algorithms, the first one is direct and the second is fast.

- **Direct algorithm**

The direct computation of a MVP: $w = Av$ can be computed by blocks. Let us consider:

$$v = (v_1, \dots, v_N) \text{ and } w = (w_1, \dots, w_N) \text{ with } v_p \in \mathbb{C}^{2M_p+1} \text{ and } w_p \in \mathbb{C}^{2M_p+1}.$$

Then, from the structure of A given by (29), we directly obtain:

$$w_l = v_l + D^p \sum_{l \le p \ne l \le N} f_l \qquad \text{with} \qquad f_l = (S^{lp})^T v_p \tag{33}$$

The computation of f_l is very costly especially when the frequency is high.

- **Fast algorithm**

Another way of computing a Toeplitz MVP for a matrix of size $n \times n$ is to use the fast algorithm explained by K. Chen [7]. In the following section we attempt to explain the main steps to achieve the fast algorithm. Now, we consider how to compute $f = T_n\, g$ quickly for a Toeplitz matrix T_n. The idea consists in building an associated circulant matrix C_m using the Toeplitz matrix T_n as follows

$$C_m = \begin{bmatrix} T_n & S_n \\ S_n & T_n \end{bmatrix}, \tag{34}$$

where

$$S_n = \begin{bmatrix} 0 & h_{n-1} & h_{n-2} & \dots & h_1 \\ h_{1-n} & 0 & h_{n-1} & \ddots & \vdots \\ h_{2-n} & \ddots & 0 & \ddots & \vdots \\ \vdots & \ddots & & & \vdots \\ h_{-1} & \dots & \dots & & 0 \end{bmatrix}$$

(35)

To compute $f = T_n\, g$, we need to define

$$\tilde{f} = C_m \tilde{g} \quad \text{and} \quad \tilde{g} = \begin{bmatrix} g \\ 0_n \end{bmatrix},$$

(36)

substituting (34) into (36) we obtain

$$\tilde{f} = \begin{bmatrix} T_n & S_n \\ S_n & T_n \end{bmatrix} \begin{bmatrix} g \\ 0_n \end{bmatrix} = \begin{bmatrix} T_n g \\ S_n g \end{bmatrix} = \begin{bmatrix} f \\ S_n g \end{bmatrix}.$$

(37)

Where 0_n denotes a zero vector of size n.

On the other hand, we have

$$\tilde{f} = F_m^{-1}[(F_m \tilde{g}).* (F_m h)].$$

(38)

Where

- F_m: is the Fast Fourier Transform (FFT).

- F_m^{-1}: is the inverse of Fast Fourier Transform (IFFT).

- h: denotes the first column of C_m.

We see clearly, from relations (37) and (38), that $f = T_n g$ is precisely the first half of vector $\tilde{f}$.

Numerically, an example is given in Fig. 11, showing the CPU time reduction in terms of wave number k using the fast MVP algorithm compared to the direct algorithm in the single-row configuration with $a_p = 1$ if p is odd and $a_p = 0.5$ if p is even $(1 \leq p \leq N), N = 20$ and $\delta = 1.5$.

5.3.3 Numerical study of the convergence rate

- **Single-row configuration**

Fig. 12 shows the dependence of the number of MVPs on the size of the scatterers. As previously seen, for this configuration $N = 15, \delta = 1$ and $k = 50$, the number of MVPs increases linearly with the obstacles radii.

For a fixed wavenumber, we also observe a dependence of MVPs with respect to the distance δ between two successive obstacles. This is observed in Fig. 13 where the number of MVPs is given according to δ in logarithmic scale for $k = 100$ and $N = 10$. We see that the number of MVPs strongly decreases as the separation distance δ tends to infinity, i.e. $\delta \gg \lambda$ (where $\lambda = \frac{2\pi}{k}$ is the wavelength). This corresponds to a weaker coupling between the obstacles in the multiple scattering phenomenon. For small values of $\delta, \delta \ll \lambda$, the number of MVPs strongly increases, because the linear system becomes ill-conditioned. Finally, we observe an intermediate resonance region for $\delta \approx \lambda$ where we have a few peaks in the number of MVPs.
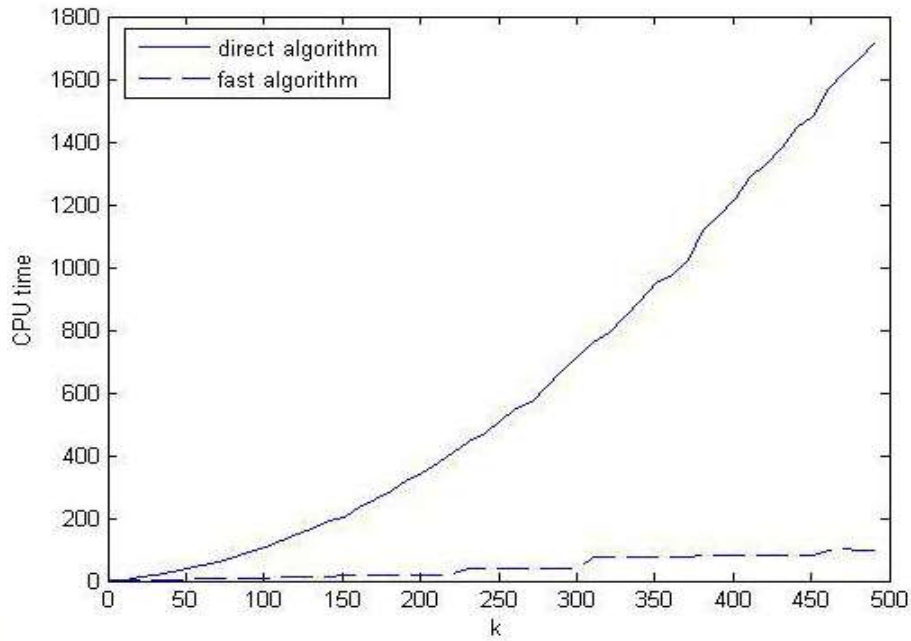
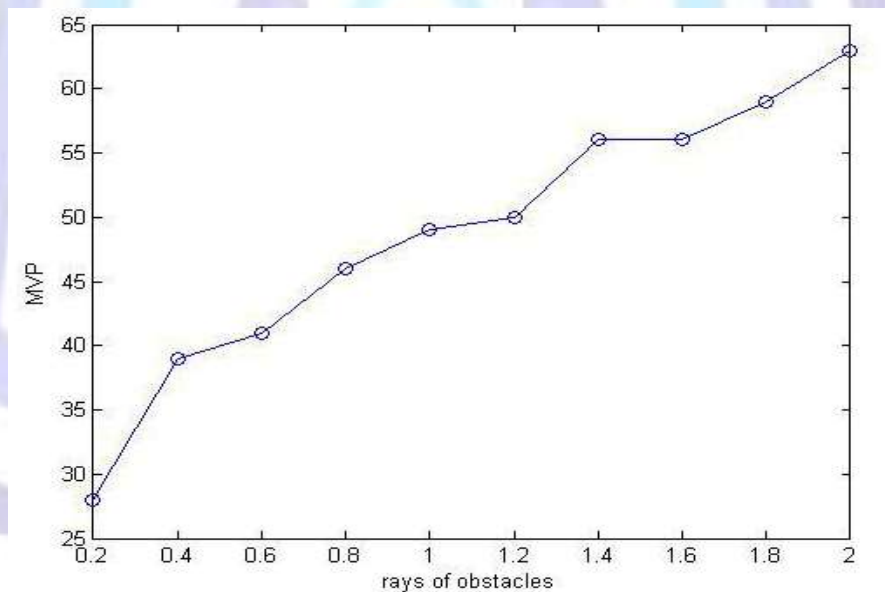**Figure 11: CPU time for calculating one Matrix-Vector product via the direct and fast algorithms (Dirichlet problem).**

Figure 12: Variation of MVPs in terms of the rays of obstacles for the single-row configuration,

$N = 15, \delta = 1, k = 50$, **GMRES(50)**, $tol = 10^{-8}$ **(Dirichlet problem).**

- **Rectangular configuration**

Now, we analyze the rectangular configuration. A first test-case is given in Fig. 14 and Fig. 15. We consider a rectangular lattice with $N_x = 5$ and $N_y = 3, \delta = 2.5$ and the rays of obstacles increase with Y direction (see configuration 1 in Fig. 14) or decrease (see configuration 2), the number of MVPs required by the GMRES(50) is represented as a function of k. In Fig. 15 we observe stabilization with the frequency but the number of MVPs increases with the thickness of layers according to the increase of obstacles radii. This is consistent with the previous observations in the single-row case.
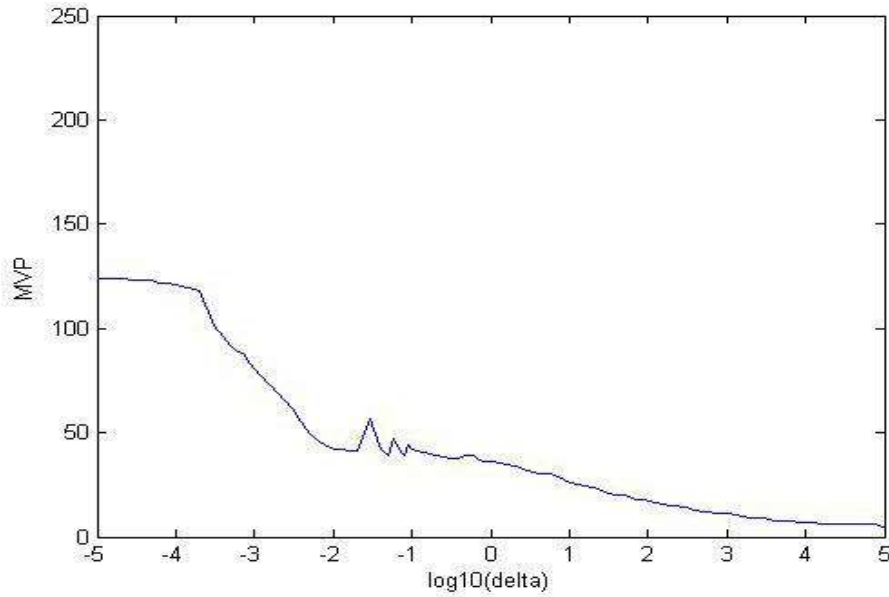
Figure 13: Variation of MVPs in terms of the distance δ separating two obstacles. We fix: $k = 100, N = 10$ obstacles, GMRES(50), $tol = 10^{-8}$ (Dirichlet problem).

A more difficult problem is considered in Fig. 16, where we represent the number of MVP with respect to the wavenumber k of a rectangular lattice with different radii $a_p = 1$ if p is odd and $a_p = 0.5$ if p is even $(1 \leq p \leq N)$ for a fixed $N_x = 5$ and different values of N_y. We observe that the number of MVPs is again slightly dependent on k but strongly varies with the number of scatterers N_y, characterizing the size of layers, and thus, with N.
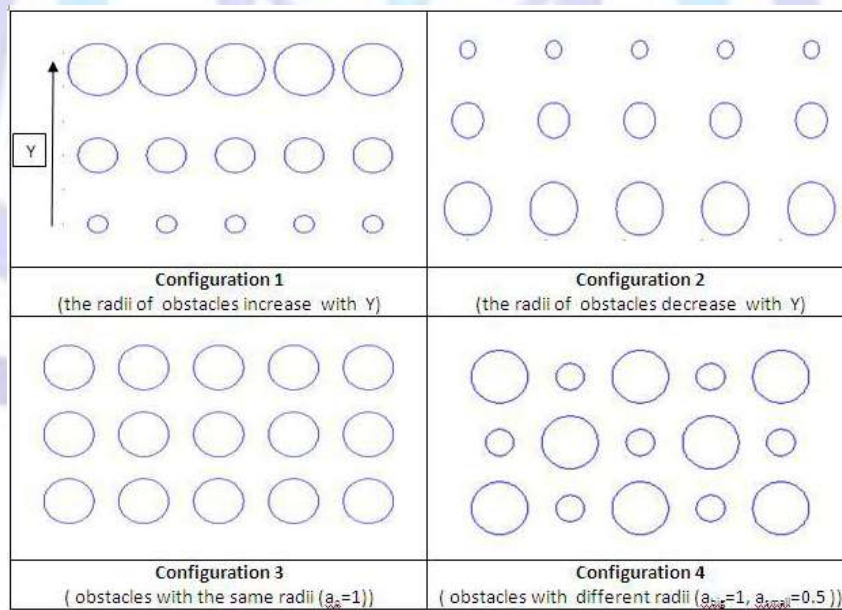

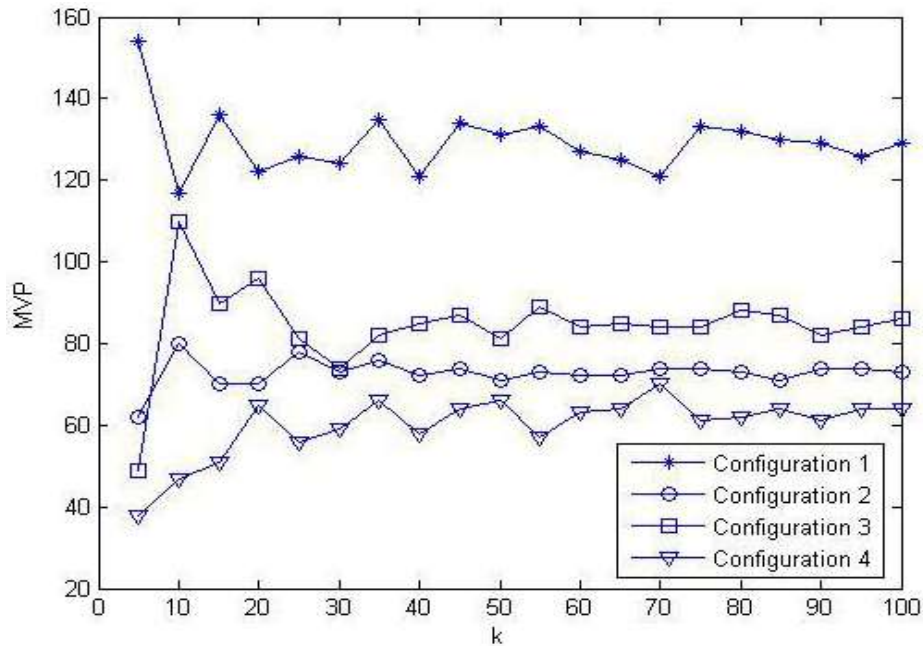**Figure 14: Rectangular configurations with different distribution.**

Figure 15: Variation of MVPs in terms of the wavenumber k for different rectangular configurations. We fix: $N_x = 5$, $N_y = 3$, $\delta = 2.5$, **GMRES(50),** $tol = 10^{-8}$ **(Dirichlet problem).**
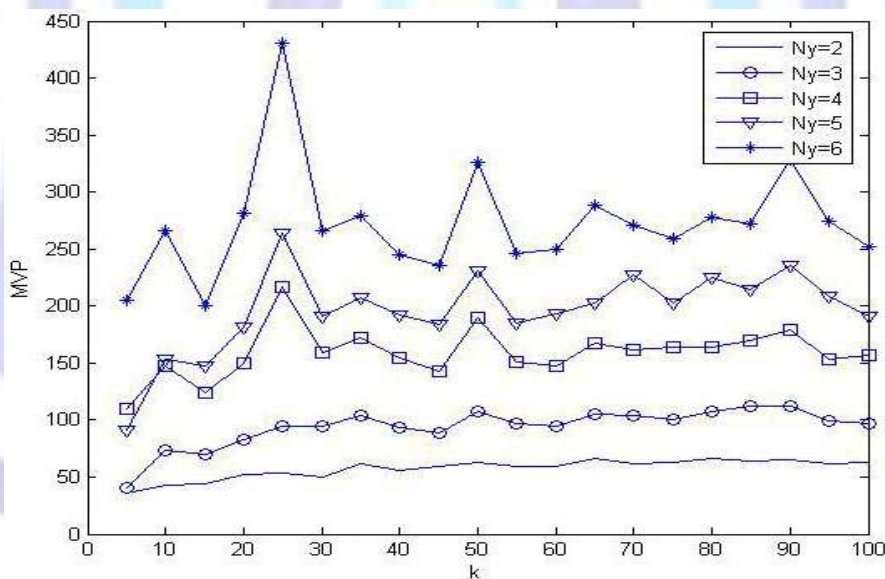

Figure 16: Variation of MVPs in terms of the wavenumber k for rectangular configuration. We fix: $N_x = 5$, $N_y = 2, ..., 6$, $\delta = 1.5$, **GMRES(50),** $tol = 10^{-8}$ **(Dirichlet problem).**

6. CONCLUSION

In this paper, we investigated the numerical simulation of high frequency multiple scattering by circular scatterers. The main difficulty in this context being the complex dense linear system to be solved which is very large and ill-conditioned. This is in particular true when the number of obstacles is large and the frequencies are high. Taking advantage of the particular block Toeplitz structure of the matrix of the linear system, we proposed an adapted storage of the system and an iterative algorithm of resolution, based on a fast MVP computation. Finally, we presented a numerical study of the convergence rate with respect to different geometrical parameters of the problem (the wavenumber, the configuration of scatterers, the distance, the radii and the number of obstacles).

REFERENCES

[1] X. Antoine, C. Chniti, K. Ramdani, On the numerical approximation of high-frequency acoustic multiple scattering problems by circular cylinders, Journal of Computational Physics 227 (2008) 1754-1771.

[2] M. Balabane, Boundary Decomposition for Helmholtz and Maxwell Equations. I. Disjoint sub-scatterers, Asymptot. Anal. 38 (1) (2004) 1-10.

[3] O. Bruno, C. Geuzaine, F. Reitich, A new high-order high-frequency integral equation method for the solution of scattering problems, II: Multiple-scattering configurations, in: Proceedings of 2004 ACES Conference},1CES, (2004).

[4] O. Bruno, C. Geuzaine, J. Monroe, F. Reitich, Prescribed error tolerances within fixed computational times for scattering problems of arbitrarily high-frequency: the convex case, Phil. Trans. R. Soc. Lond. 362 (2004) 625-649.

[5] W.H. Butler, P.H. Dederichs, A. Gonis, R.L. Weaver(eds.), Applications of Multiple Scattering Theory to Materials Science. Pittsburgh: Materials Research Society, (1992).

[6] Q. Carayol, F. Collino, Error Estimates in the Fast Multipole Method for Scattering Problems. Part 1: Truncation of the Jacobi-Anger series, M2AN 38 (2) (2004) 371-394.

[7] K. Chen, Matrix Preconditioning, Techniques and Applications, Cambridge Monographs on Applied and Computational Mathematics, (2005).

[8] W.C. Chen, J.M. Jin, E. Michielssen, J. Song, Fast and Efficient Algorithms in Computational Electromagnetics, Artech House Antennas and Propagation Library, Norwood, (2001).

[9] F. Ecevit, F. Reitich, Analysis of multiple scattering interactions for high-frequency scattering problems. I: The twodimensional case, Preprint, School of Mathematics, University of Minnesota, (2006).

[10] B.V. Genechten, B. Bergen, D. Vandepitte, W. Desmet, A Trefftz-based numerical modelling framework for Helmholtz problems with complex multiple-scatterer configurations, Journal of Computational Physics 229 (2000) 6623-6643.

[11] A. Gonis, Green Functions for Ordered and Disordred Systems. Amsterdam: North-Holland, (1992).

[12] A. Gonis, Theoretical Materials Science. Warrendale: Materials Research society, (2000).

[13] A. Gonis, W.H. Butler, Multiple scattering in solids. New York: Springer, (2000).

[14] N.A. Gumerov, R. Duraiswami, Multiple scattering from N spheres using multipole re-expansion, J. Acoust. Soc. Am. 112 (2002) 2688-2701.

[15] R.J. Hanson, D.R. Kincaid, Notes on GMRES Algorithm Organization, Technical Report TR-05-05, (2005).

[16] P.A. Martin, Multiple Scattering, Interaction of Time-Harmonic Waves with N obstacles, Encyclopedia of Mathematics and its Appliction 107, Cambridge, (2006).

[17] Y. Saad, Iterative Methods for Sparse Linear Systems 2nd Edition. SIAM, Philadelphia, (2003).

[18] Y. Saad, Iterative Methods for Sparse Linear Systems, PWS Pub. Co., Boston, (1996).

[19] L. Tsang, J.A. Kong, K.H. Ding, C.O. Ao, Scattering of Electromagnetic Waves, Numerical Simulation, in: J.A. Kong(Ed.), Wiley Series in Remote Sensing, (2001).

[20] O. Yilmaz, An iterative procedure for the diffraction problem of water waves by multiple cylinders, Ocean Eng.31 (24) (2004) 1437-1446.

[21] O. Yilmaz, A. Incecik, N. Barltrop, Wave enhancement due to blockage in semi-submersible and TLP structures, Ocean Eng. 28 (2001) 471-490.

[22] F. Zaviska, Uber die Beugeng elektromagnetischer Wellen an parallelen, unendlich langen Kreiszylindern, Annalen der Physik, 4 Folge 40 (1913) 1023-1056.

[23] Y.J. Zhang, E.P. Li, Fast multipole scattering matrix method for multiple scattering of a large number of cylinders, PIER 72 (2007) 105-126.